Study of the decays $D_s^+ \to K_S^0 K^+$ and $K_L^0 K^+$

M. Ablikim,[1] M. N. Achasov,[10,d] P. Adlarson,[59] S. Ahmed,[15] M. Albrecht,[4] M. Alekseev,[58a,58c] A. Amoroso,[58a,58c] F. F. An,[1] Q. An,[55,43] Y. Bai,[42] O. Bakina,[27] R. Baldini Ferroli,[23a] I. Balossino,[24a] Y. Ban,[35] K. Begzsuren,[25] J. V. Bennett,[5] N. Berger,[26] M. Bertani,[23a] D. Bettoni,[24a] F. Bianchi,[58a,58c] J. Biernat,[59] J. Bloms,[52] I. Boyko,[27] R. A. Briere,[5] H. Cai,[60] X. Cai,[1,43] A. Calcaterra,[23a] G. F. Cao,[1,47] N. Cao,[1,47] S. A. Cetin,[46b] J. Chai,[58c] J. F. Chang,[1,43] W. L. Chang,[1,47] G. Chelkov,[27,b,c] D. Y. Chen,[6] G. Chen,[1] H. S. Chen,[1,47] J. C. Chen,[1] M. L. Chen,[1,43] S. J. Chen,[33] Y. B. Chen,[1,43] W. Cheng,[58c] G. Cibinetto,[24a] F. Cossio,[58c] X. F. Cui,[34] H. L. Dai,[1,43] J. P. Dai,[38,h] X. C. Dai,[1,47] A. Dbeyssi,[15] D. Dedovich,[27] Z. Y. Deng,[1] A. Denig,[26] I. Denysenko,[27] M. Destefanis,[58a,58c] F. De Mori,[58a,58c] Y. Ding,[31] C. Dong,[34] J. Dong,[1,43] L. Y. Dong,[1,47] M. Y. Dong,[1,43,47] Z. L. Dou,[33] S. X. Du,[63] J. Z. Fan,[45] J. Fang,[1,43] S. S. Fang,[1,47] Y. Fang,[1] R. Farinelli,[24a,24b] L. Fava,[58b,58c] F. Feldbauer,[4] G. Felici,[23a] C. Q. Feng,[55,43] M. Fritsch,[4] C. D. Fu,[1] Y. Fu,[1] Q. Gao,[1] X. L. Gao,[55,43] Y. Gao,[45] Y. Gao,[56] Y. G. Gao,[6] Z. Gao,[55,43] B. Garillon,[26] I. Garzia,[24a] E. M. Gersabeck,[50] A. Gilman,[51] K. Goetzen,[11] L. Gong,[34] W. X. Gong,[1,43] W. Gradl,[26] M. Greco,[58a,58c] L. M. Gu,[33] M. H. Gu,[1,43] S. Gu,[2] Y. T. Gu,[13] A. Q. Guo,[22] L. B. Guo,[32] R. P. Guo,[36] Y. P. Guo,[26] A. Guskov,[27] S. Han,[60] X. Q. Hao,[16] F. A. Harris,[48] K. L. He,[1,47] F. H. Heinsius,[4] T. Held,[4] Y. K. Heng,[1,43,47] M. Himmelreich,[11,g] Y. R. Hou,[47] Z. L. Hou,[1] H. M. Hu,[1,47] J. F. Hu,[38,h] T. Hu,[1,43,47] Y. Hu,[1] G. S. Huang,[55,43] J. S. Huang,[16] X. T. Huang,[37] X. Z. Huang,[33] N. Huesken,[52] T. Hussain,[57] W. Ikegami Andersson,[59] W. Imoehl,[22] M. Irshad,[55,43] Q. Ji,[1] Q. P. Ji,[16] X. B. Ji,[1,47] X. L. Ji,[1,43] H. L. Jiang,[37] X. S. Jiang,[1,43,47] X. Y. Jiang,[34] J. B. Jiao,[37] Z. Jiao,[18] D. P. Jin,[1,43,47] S. Jin,[33] Y. Jin,[49] T. Johansson,[59] N. Kalantar-Nayestanaki,[29] X. S. Kang,[31] R. Kappert,[29] M. Kavatsyuk,[29] B. C. Ke,[1] I. K. Keshk,[4] A. Khoukaz,[52] P. Kiese,[26] R. Kiuchi,[1] R. Kliemt,[11] L. Koch,[28] O. B. Kolcu,[46b,f] B. Kopf,[4] M. Kuemmel,[4] M. Kuessner,[4] A. Kupsc,[59] M. Kurth,[1] M. G. Kurth,[1,47] W. Kühn,[28] J. S. Lange,[28] P. Larin,[15] L. Lavezzi,[58c] H. Leithoff,[26] T. Lenz,[26] C. Li,[59] Cheng Li,[55,43] D. M. Li,[63] F. Li,[1,43] F. Y. Li,[35] G. Li,[1] H. B. Li,[1,47] H. J. Li,[9,j] J. C. Li,[1] J. W. Li,[41] Ke Li,[1] L. K. Li,[1] Lei Li,[3] P. L. Li,[55,43] P. R. Li,[30] Q. Y. Li,[37] W. D. Li,[1,47] W. G. Li,[1] X. H. Li,[55,43] X. L. Li,[37] X. N. Li,[1,43] Z. B. Li,[44] Z. Y. Li,[44] H. Liang,[55,43] H. Liang,[1,47] Y. F. Liang,[40] Y. T. Liang,[28] G. R. Liao,[12] L. Z. Liao,[1,47] J. Libby,[21] C. X. Lin,[44] D. X. Lin,[15] Y. J. Lin,[13] B. Liu,[38,h] B. J. Liu,[1] C. X. Liu,[1] D. Liu,[55,43] D. Y. Liu,[38,h] F. H. Liu,[39] Fang Liu,[1] Feng Liu,[6] H. B. Liu,[13] H. M. Liu,[1,47] Huanhuan Liu,[1] Huihui Liu,[17] J. B. Liu,[55,43] J. Y. Liu,[1,47] K. Y. Liu,[31] Ke Liu,[6] L. Y. Liu,[13] Q. Liu,[47] S. B. Liu,[55,43] T. Liu,[1,47] X. Liu,[30] X. Y. Liu,[1,47] Y. B. Liu,[34] Z. A. Liu,[1,43,47] Zhiqing Liu,[37] Y. F. Long,[35] X. C. Lou,[1,43,47] H. J. Lu,[18] J. D. Lu,[1,47] J. G. Lu,[1,43] Y. Lu,[1] Y. P. Lu,[1,43] C. L. Luo,[32] M. X. Luo,[62] P. W. Luo,[44] T. Luo,[9,j] X. L. Luo,[1,43] S. Lusso,[58c] X. R. Lyu,[47] F. C. Ma,[31] H. L. Ma,[1] L. L. Ma,[37] M. M. Ma,[1,47] Q. M. Ma,[1] X. N. Ma,[34] X. X. Ma,[1,47] X. Y. Ma,[1,43] Y. M. Ma,[37] F. E. Maas,[15] M. Maggiora,[58a,58c] S. Maldaner,[26] S. Malde,[53] Q. A. Malik,[57] A. Mangoni,[23b] Y. J. Mao,[35] Z. P. Mao,[1] S. Marcello,[58a,58c] Z. X. Meng,[49] J. G. Messchendorp,[29] G. Mezzadri,[24a] J. Min,[1,43] T. J. Min,[33] R. E. Mitchell,[22] X. H. Mo,[1,43,47] Y. J. Mo,[6] C. Morales Morales,[15] N. Yu. Muchnoi,[10,d] H. Muramatsu,[51] A. Mustafa,[4] S. Nakhoul,[11,g] Y. Nefedov,[27] F. Nerling,[11,g] I. B. Nikolaev,[10,d] Z. Ning,[1,43] S. Nisar,[8,k] S. L. Niu,[1,43] S. L. Olsen,[47] Q. Ouyang,[1,43,47] S. Pacetti,[23b] Y. Pan,[55,43] M. Papenbrock,[59] P. Patteri,[23a] M. Pelizaeus,[4] H. P. Peng,[55,43] K. Peters,[11,g] J. Pettersson,[59] J. L. Ping,[32] R. G. Ping,[1,47] A. Pitka,[4] R. Poling,[51] V. Prasad,[55,43] M. Qi,[33] T. Y. Qi,[2] S. Qian,[1,43] C. F. Qiao,[47] N. Qin,[60] X. P. Qin,[13] X. S. Qin,[4] Z. H. Qin,[1,43] J. F. Qiu,[1] S. Q. Qu,[34] K. H. Rashid,[57,i] K. Ravindran,[21] C. F. Redmer,[26] M. Richter,[4] A. Rivetti,[58c] V. Rodin,[29] M. Rolo,[58c] G. Rong,[1,47] Ch. Rosner,[15] M. Rump,[52] A. Sarantsev,[27,e] Y. Schelhaas,[26] K. Schoenning,[59] W. Shan,[19] X. Y. Shan,[55,43,*] M. Shao,[55,43] C. P. Shen,[2] P. X. Shen,[34] X. Y. Shen,[1,47] H. Y. Sheng,[1] X. Shi,[1,43] X. D. Shi,[55,43] J. J. Song,[37] Q. Q. Song,[55,43] X. Y. Song,[1] S. Sosio,[58a,58c] C. Sowa,[4] S. Spataro,[58a,58c] F. F. Sui,[37] G. X. Sun,[1] J. F. Sun,[16] L. Sun,[60] S. S. Sun,[1,47] X. H. Sun,[1] Y. J. Sun,[55,43] Y. K. Sun,[55,43] Y. Z. Sun,[1] Z. J. Sun,[1,43] Z. T. Sun,[1] Y. T. Tan,[55,43] C. J. Tang,[40] G. Y. Tang,[1] X. Tang,[1] V. Thoren,[59] B. Tsednee,[25] I. Uman,[46d] B. Wang,[1] B. L. Wang,[47] C. W. Wang,[33] D. Y. Wang,[35] K. Wang,[1,43] L. L. Wang,[1] L. S. Wang,[1] M. Wang,[37] M. Z. Wang,[35] Meng Wang,[1,47] P. L. Wang,[1] R. M. Wang,[61] W. P. Wang,[55,43] X. Wang,[35] X. F. Wang,[1] X. L. Wang,[9,j] Y. Wang,[55,43] Y. Wang,[44] Y. F. Wang,[1,43,47] Z. Wang,[1,43] Z. G. Wang,[1,43] Z. Y. Wang,[1] Zongyuan Wang,[1,47] T. Weber,[4] D. H. Wei,[12] P. Weidenkaff,[26] H. W. Wen,[32] S. P. Wen,[1] U. Wiedner,[4] G. Wilkinson,[53] M. Wolke,[59] L. H. Wu,[1] L. J. Wu,[1,47] Z. Wu,[1,43] L. Xia,[55,43] Y. Xia,[20] S. Y. Xiao,[1] Y. J. Xiao,[1,47] Z. J. Xiao,[32] Y. G. Xie,[1,43] Y. H. Xie,[6] T. Y. Xing,[1,47] X. A. Xiong,[1,47] Q. L. Xiu,[1,43] G. F. Xu,[1] J. J. Xu,[33] L. Xu,[1] Q. J. Xu,[14] W. Xu,[1,47] X. P. Xu,[41] F. Yan,[56] L. Yan,[58a,58c] W. B. Yan,[55,43] W. C. Yan,[2] Y. H. Yan,[20] H. J. Yang,[38,h] H. X. Yang,[1] L. Yang,[60] R. X. Yang,[55,43] S. L. Yang,[1,47] Y. H. Yang,[33] Y. X. Yang,[12] Yifan Yang,[1,47] Z. Q. Yang,[20] M. Ye,[1,43] M. H. Ye,[7] J. H. Yin,[1] Z. Y. You,[44] B. X. Yu,[1,43,47] C. X. Yu,[34] J. S. Yu,[20] T. Yu,[56] C. Z. Yuan,[1,47] X. Q. Yuan,[35] Y. Yuan,[1] A. Yuncu,[46b,a] A. A. Zafar,[57] Y. Zeng,[20] B. X. Zhang,[1] B. Y. Zhang,[1,43] C. C. Zhang,[1] D. H. Zhang,[1] H. H. Zhang,[44] H. Y. Zhang,[1,43] J. Zhang,[1,47] J. L. Zhang,[61] J. Q. Zhang,[4]

J. W. Zhang,[1,43,47] J. Y. Zhang,[1] J. Z. Zhang,[1,47] K. Zhang,[1,47] L. Zhang,[45] S. F. Zhang,[33] T. J. Zhang,[38,h] X. Y. Zhang,[37] Y. Zhang,[55,43] Y. H. Zhang,[1,43] Y. T. Zhang,[55,43] Yang Zhang,[1] Yao Zhang,[1] Yi Zhang,[9,j] Yu Zhang,[47] Z. H. Zhang,[6] Z. P. Zhang,[55] Z. Y. Zhang,[60] G. Zhao,[1] J. W. Zhao,[1,43] J. Y. Zhao,[1,47] J. Z. Zhao,[1,43] Lei Zhao,[55,43] Ling Zhao,[1] M. G. Zhao,[34] Q. Zhao,[1] S. J. Zhao,[63] T. C. Zhao,[1] Y. B. Zhao,[1,43] Z. G. Zhao,[55,43] A. Zhemchugov,[27,b] B. Zheng,[56] J. P. Zheng,[1,43] Y. Zheng,[35] Y. H. Zheng,[47] B. Zhong,[32] L. Zhou,[1,43] L. P. Zhou,[1,47] Q. Zhou,[1,47] X. Zhou,[60] X. K. Zhou,[47] X. R. Zhou,[55,43] Xiaoyu Zhou,[20] Xu Zhou,[20] A. N. Zhu,[1,47] J. Zhu,[34] J. Zhu,[44] K. Zhu,[1] K. J. Zhu,[1,43,47] S. H. Zhu,[54] W. J. Zhu,[34] X. L. Zhu,[45] Y. C. Zhu,[55,43] Y. S. Zhu,[1,47] Z. A. Zhu,[1,47] J. Zhuang,[1,43] B. S. Zou,[1] and J. H. Zou[1]

(BESIII Collaboration)

[1]*Institute of High Energy Physics, Beijing 100049, People's Republic of China*
[2]*Beihang University, Beijing 100191, People's Republic of China*
[3]*Beijing Institute of Petrochemical Technology, Beijing 102617, People's Republic of China*
[4]*Bochum Ruhr-University, D-44780 Bochum, Germany*
[5]*Carnegie Mellon University, Pittsburgh, Pennsylvania 15213, USA*
[6]*Central China Normal University, Wuhan 430079, People's Republic of China*
[7]*China Center of Advanced Science and Technology, Beijing 100190, People's Republic of China*
[8]*COMSATS University Islamabad, Lahore Campus, Defence Road, Off Raiwind Road, 54000 Lahore, Pakistan*
[9]*Fudan University, Shanghai 200443, People's Republic of China*
[10]*G.I. Budker Institute of Nuclear Physics SB RAS (BINP), Novosibirsk 630090, Russia*
[11]*GSI Helmholtzcentre for Heavy Ion Research GmbH, D-64291 Darmstadt, Germany*
[12]*Guangxi Normal University, Guilin 541004, People's Republic of China*
[13]*Guangxi University, Nanning 530004, People's Republic of China*
[14]*Hangzhou Normal University, Hangzhou 310036, People's Republic of China*
[15]*Helmholtz Institute Mainz, Johann-Joachim-Becher-Weg 45, D-55099 Mainz, Germany*
[16]*Henan Normal University, Xinxiang 453007, People's Republic of China*
[17]*Henan University of Science and Technology, Luoyang 471003, People's Republic of China*
[18]*Huangshan College, Huangshan 245000, People's Republic of China*
[19]*Hunan Normal University, Changsha 410081, People's Republic of China*
[20]*Hunan University, Changsha 410082, People's Republic of China*
[21]*Indian Institute of Technology Madras, Chennai 600036, India*
[22]*Indiana University, Bloomington, Indiana 47405, USA*
[23a]*INFN Laboratori Nazionali di Frascati, I-00044 Frascati, Italy*
[23b]*INFN and University of Perugia, I-06100 Perugia, Italy*
[24a]*INFN Sezione di Ferrara, I-44122 Ferrara, Italy*
[24b]*University of Ferrara, I-44122 Ferrara, Italy*
[25]*Institute of Physics and Technology, Peace Ave. 54B, Ulaanbaatar 13330, Mongolia*
[26]*Johannes Gutenberg University of Mainz, Johann-Joachim-Becher-Weg 45, D-55099 Mainz, Germany*
[27]*Joint Institute for Nuclear Research, 141980 Dubna, Moscow Region, Russia*
[28]*Justus-Liebig-Universitaet Giessen, II. Physikalisches Institut, Heinrich-Buff-Ring 16, D-35392 Giessen, Germany*
[29]*KVI-CART, University of Groningen, NL-9747 AA Groningen, The Netherlands*
[30]*Lanzhou University, Lanzhou 730000, People's Republic of China*
[31]*Liaoning University, Shenyang 110036, People's Republic of China*
[32]*Nanjing Normal University, Nanjing 210023, People's Republic of China*
[33]*Nanjing University, Nanjing 210093, People's Republic of China*
[34]*Nankai University, Tianjin 300071, People's Republic of China*
[35]*Peking University, Beijing 100871, People's Republic of China*
[36]*Shandong Normal University, Jinan 250014, People's Republic of China*
[37]*Shandong University, Jinan 250100, People's Republic of China*
[38]*Shanghai Jiao Tong University, Shanghai 200240, People's Republic of China*
[39]*Shanxi University, Taiyuan 030006, People's Republic of China*
[40]*Sichuan University, Chengdu 610064, People's Republic of China*
[41]*Soochow University, Suzhou 215006, People's Republic of China*
[42]*Southeast University, Nanjing 211100, People's Republic of China*
[43]*State Key Laboratory of Particle Detection and Electronics, Beijing 100049, Hefei 230026, People's Republic of China*

[44]Sun Yat-Sen University, Guangzhou 510275, People's Republic of China
[45]Tsinghua University, Beijing 100084, People's Republic of China
[46a]Ankara University, 06100 Tandogan, Ankara, Turkey
[46b]Istanbul Bilgi University, 34060 Eyup, Istanbul, Turkey
[46c]Uludag University, 16059 Bursa, Turkey
[46d]Near East University, Nicosia, North Cyprus, Mersin 10, Turkey
[47]University of Chinese Academy of Sciences, Beijing 100049, People's Republic of China
[48]University of Hawaii, Honolulu, Hawaii 96822, USA
[49]University of Jinan, Jinan 250022, People's Republic of China
[50]University of Manchester, Oxford Road, Manchester M13 9PL, United Kingdom
[51]University of Minnesota, Minneapolis, Minnesota 55455, USA
[52]University of Muenster, Wilhelm-Klemm-Straße 9, 48149 Muenster, Germany
[53]University of Oxford, Keble Road, Oxford OX13RH, United Kingdom
[54]University of Science and Technology Liaoning, Anshan 114051, People's Republic of China
[55]University of Science and Technology of China, Hefei 230026, People's Republic of China
[56]University of South China, Hengyang 421001, People's Republic of China
[57]University of the Punjab, Lahore 54590, Pakistan
[58a]University of Turin, I-10125 Turin, Italy
[58b]University of Eastern Piedmont, I-15121 Alessandria, Italy
[58c]INFN, I-10125 Turin, Italy
[59]Uppsala University, Box 516, SE-75120 Uppsala, Sweden
[60]Wuhan University, Wuhan 430072, People's Republic of China
[61]Xinyang Normal University, Xinyang 464000, People's Republic of China
[62]Zhejiang University, Hangzhou 310027, People's Republic of China
[63]Zhengzhou University, Zhengzhou 450001, People's Republic of China

(Received 11 March 2019; published 12 June 2019)

Using an e^+e^- annihilation data sample corresponding to an integrated luminosity of 3.19 fb^{-1} and collected at a center-of-mass energy $\sqrt{s} = 4.178$ GeV with the BESIII detector, we measure the absolute branching fractions $\mathcal{B}(D_s^+ \to K_S^0 K^+) = (1.425 \pm 0.038_{\text{stat.}} \pm 0.031_{\text{syst.}})\%$ and $\mathcal{B}(D_s^+ \to K_L^0 K^+) = (1.485 \pm 0.039_{\text{stat.}} \pm 0.046_{\text{syst.}})\%$. The branching fraction of $D_s^+ \to K_S^0 K^+$ is compatible with the world average and that of $D_s^+ \to K_L^0 K^+$ is measured for the first time. We present the first measurement of the K_S^0-K_L^0 asymmetry in the decays $D_s^+ \to K_{S,L}^0 K^+$, and $R(D_s^+ \to K_{S,L}^0 K^+) = \frac{\mathcal{B}(D_s^+ \to K_S^0 K^+) - \mathcal{B}(D_s^+ \to K_L^0 K^+)}{\mathcal{B}(D_s^+ \to K_S^0 K^+) + \mathcal{B}(D_s^+ \to K_L^0 K^+)} = (-2.1 \pm 1.9_{\text{stat.}} \pm 1.6_{\text{syst.}})\%$. In addition, we measure the direct CP asymmetries $A_{CP}(D_s^\pm \to K_S^0 K^\pm) = (0.6 \pm 2.8_{\text{stat.}} \pm 0.6_{\text{syst.}})\%$ and $A_{\text{CP}}(D_s^\pm \to K_L^0 K^\pm) = (-1.1 \pm 2.6_{\text{stat.}} \pm 0.6_{\text{syst.}})\%$.

DOI: 10.1103/PhysRevD.99.112005

*Corresponding author.
shanxy@mail.ustc.edu.cn
[a]Also at Bogazici University, 34342 Istanbul, Turkey.
[b]Also at the Moscow Institute of Physics and Technology, Moscow 141700, Russia.
[c]Also at the Functional Electronics Laboratory, Tomsk State University, Tomsk 634050, Russia.
[d]Also at the Novosibirsk State University, Novosibirsk 630090, Russia.
[e]Also at the NRC "Kurchatov Institute," PNPI, Gatchina 188300, Russia.
[f]Also at Istanbul Arel University, 34295 Istanbul, Turkey.
[g]Also at Goethe University Frankfurt, 60323 Frankfurt am Main, Germany.
[h]Also at Key Laboratory for Particle Physics, Astrophysics and Cosmology, Ministry of Education; Shanghai Key Laboratory for Particle Physics and Cosmology; Institute of Nuclear and Particle Physics, Shanghai 200240, People's Republic of China.
[i]Also at Government College Women University, Sialkot—51310, Punjab, Pakistan.
[j]Also at Key Laboratory of Nuclear Physics and Ion-beam Application (MOE) and Institute of Modern Physics, Fudan University, Shanghai 200443, People's Republic of China.
[k]Also at Harvard University, Department of Physics, Cambridge, Massachusetts 02138, USA.

I. INTRODUCTION

Two-body hadronic decays of charmed mesons, $D \to P_1P_2$ (where $P_{1,2}$ denotes a pseudoscalar meson), serve as an ideal environment to improve our understanding of the weak and strong interactions because of their relatively simple topology [1,2]. Charmed-meson decays into hadronic final states that contain a neutral kaon are particularly attractive. Bigi and Yamamoto [3] first pointed out that the interference of the decay amplitudes of the Cabibbo-favored (CF) transition $D \to \bar{K}^0\pi$ and the doubly-Cabibbo-suppressed (DCS) transition $D \to K^0\pi$ can result in a measurable $K^0_S - K^0_L$ asymmetry

$$R(D \to K^0_{S,L}\pi) = \frac{\mathcal{B}(D \to K^0_S\pi) - \mathcal{B}(D \to K^0_L\pi)}{\mathcal{B}(D \to K^0_S\pi) + \mathcal{B}(D \to K^0_L\pi)}. \quad (1)$$

A similar asymmetry can be defined in D^+_s decays by replacing π with K. Additionally, as pointed out in Ref. [4], the interference between CF and DCS amplitudes can also lead to a new CP violation effect, which is estimated to be of an order of 10^{-3}. The measurement of K^0_S-K^0_L asymmetries and CP asymmetries in charmed-meson decays with a neutral kaon provides insight into the DCS process, as well as information to explore D^0-$\bar{D}^0$ mixing, CP violation and SU(3) flavor-symmetry breaking effects in the charm sector [5,6].

On the theory side, there are different phenomenological models which give predictions for the K^0_S-K^0_L asymmetries, such as: the topological-diagrammatic approach [2] under the SU(3) flavor symmetry (DIAG) or incorporating the SU(3) breaking effects [$\mathrm{SU(3)_{FB}}$] [7–9], the QCD factorization approach (QCDF) [10], and the factorization-assisted topological-amplitude (FAT) [11]. The predicted $K^0_S - K^0_L$ asymmetries in charmed-meson decays from these different approaches, as well as the measured values reported by the CLEO Collaboration [12], are summarized in Table I. Considering the large range of values predicted for the K^0_S-K^0_L asymmetries, their measurements provide a crucial constraint upon models of the dynamics of charmed meson decays.

Experimentally, $D^{+(0)}$ decays have been studied intensively in the past two decades [13]. However, existing measurements of charmed-strange meson decays suffer from poor precision due to the limited size of available data samples and a relatively small production cross section in e^+e^- annihilation [14]. The most recent measurement of $\mathcal{B}(D^+_s \to K^0_S K^+) = (1.52 \pm 0.05_{\mathrm{stat.}} \pm 0.03_{\mathrm{syst.}})\%$ was reported by the CLEO Collaboration [15]; the result was obtained using a global fit to multiple decay modes reconstructed in an e^+e^- annihilation sample corresponding to an integrated luminosity of 586 pb^{-1} at a center-of-mass energy $\sqrt{s} = 4.17$ GeV. The Belle Collaboration reported a measurement of the branching fraction $\mathcal{B}(D^+_s \to \bar{K}^0K^+)$ (ignoring the contribution from K^0K) [16] using a data sample corresponding to an integrated luminosity of 913 fb^{-1} collected at $\sqrt{s}$ around the $\Upsilon(4S)$ and $\Upsilon(5S)$ resonances. Neither $\mathcal{B}(D^+_s \to K^0_L K^+)$ nor the corresponding K^0_S-K^0_L asymmetry have been measured yet.

In this paper, measurements of the absolute branching fractions for the decays $D^+_s \to K^0_S K^+$ and $D^+_s \to K^0_L K^+$, the K^0_S-K^0_L asymmetry, and the corresponding CP asymmetries are performed using a sample of e^+e^- annihilation data collected at $\sqrt{s} = 4.178$ GeV with the BESIII detector at the BEPCII. The data sample corresponds to an integrated luminosity of 3.19 fb^{-1}. Throughout the paper, charge conjugation modes are implicitly implied, unless otherwise noted.

II. BESIII DETECTOR AND MONTE CARLO SIMULATION

The BESIII detector is a magnetic spectrometer that operates at the BEPCII e^+e^- collider [17]. The detector has a cylindrical geometry that covers 93% of the 4π solid angle and consists of several subdetectors. A main drift chamber (MDC) with 43 layers surrounding the beam pipe measures momenta and specific ionization of charged particles. Plastic scintillator time of flight counters (TOF), located outside of the MDC, provide charged-particle identification information, and an electromagnetic calorimeter (EMC), consisting of 6240 CsI(Tl) crystals, detects electromagnetic showers. These subdetectors are immersed in a magnetic field of 1 T, produced by a superconducting solenoid, and are surrounded by a multilayered resistive-plate chamber (RPC) system interleaved in the steel flux return of the solenoid, providing muon identification. In 2015, BESIII was upgraded by replacing the two end-cap TOF systems with multigap RPCs, which achieve a time resolution of 60 ps [18]. A detailed description of the BESIII detector is presented in Ref. [19].

TABLE I. Predictions for K^0_S-K^0_L asymmetries in charmed-meson decays from different phenomenological models and the CLEO measurements.

	DIAG [7]	DIAG [8]	QCDF [10]	$\mathrm{SU(3)_{FB}}$ [9]	FAT [11]	CLEO [12]
$R(D^0 \to K^0_{S,L}\pi^0)(\%)$	10.7	10.7	10.6	9^{+4}_{-2}	11.3 ± 0.1	$10.8 \pm 2.5_{\mathrm{stat.}} \pm 2.4_{\mathrm{syst.}}$
$R(D^+ \to K^0_{S,L}\pi^+)(\%)$	-0.5 ± 1.3	-1.9 ± 1.6	-1.0 ± 2.6	⋯	2.5 ± 0.8	$2.2 \pm 1.6_{\mathrm{stat.}} \pm 1.8_{\mathrm{syst.}}$
$R(D^+_s \to K^0_{S,L}K^+)(\%)$	-0.22 ± 0.87	-0.8 ± 0.7	-0.8 ± 0.7	11^{+4}_{-14}	1.2 ± 0.6	⋯

TABLE II. Summary of the D_s^- ST yields, along with the ST and DT detection efficiencies for that decay mode. The uncertainty is statistical only. The decay branching fractions of subsequent decays in the ST side are not included in the efficiencies. The decay branching fraction of $K_S^0 \to \pi^+\pi^-$ in the signal side is included in $\epsilon_{\rm DT}^{K_S^0}$.

Tag mode	$N_{\rm ST}$	$\epsilon_{\rm ST}$ (%)	$\epsilon_{\rm DT}^{K_S^0}$ (%)	$\epsilon_{MM^2}^{K_L^0}$ (%)
$K^+K^-\pi^-$	141285 ± 631	42.15 ± 0.03	13.58 ± 0.07	16.33 ± 0.10
$K^-\pi^+\pi^-$	18051 ± 575	48.84 ± 0.26	16.35 ± 0.08	19.73 ± 0.12
$\pi^+\pi^-\pi^-$	40573 ± 964	56.05 ± 0.18	18.47 ± 0.08	22.55 ± 0.12
$K^+K^-\pi^-\pi^0$	41001 ± 840	10.61 ± 0.03	3.86 ± 0.04	5.02 ± 0.06
$\pi^-\eta'_{\gamma\rho^0}$	26360 ± 833	35.33 ± 0.16	12.41 ± 0.07	15.59 ± 0.10
$\rho^-\eta$	32922 ± 878	16.65 ± 0.06	5.99 ± 0.06	8.84 ± 0.09
$K_S^0K^-\pi^+\pi^-$	8081 ± 283	18.47 ± 0.11	6.16 ± 0.05	7.72 ± 0.07
$K_S^0K^+\pi^-\pi^-$	15331 ± 249	21.44 ± 0.06	6.82 ± 0.05	8.21 ± 0.07
$K_S^0K^-\pi^0$	11380 ± 385	16.97 ± 0.12	5.94 ± 0.05	7.82 ± 0.07
$K_S^0K_S^0\pi^-$	5015 ± 164	22.86 ± 0.11	6.95 ± 0.05	8.98 ± 0.07
$\pi^-\eta$	19050 ± 512	46.60 ± 0.19	16.06 ± 0.07	21.99 ± 0.13
$\pi^-\eta'_{\pi^+\pi^-\eta}$	7694 ± 137	18.80 ± 0.05	6.16 ± 0.05	8.45 ± 0.08
$\pi^-\eta_{\pi^+\pi^-\pi^0}$	5448 ± 169	22.30 ± 0.11	7.47 ± 0.06	9.70 ± 0.08

The performance of the BESIII detector is evaluated using a GEANT4-based [20] Monte Carlo (MC) program that includes a description of the detector geometry and simulates its response. In the MC simulation, the production of open charm processes directly produced via e^+e^- annihilation are modeled with the generator CONEXC [21], which includes the effects of the beam energy spread and initial-state radiation (ISR). The ISR production of vector charmonium states [$\psi(3770)$, $\psi(3686)$ and J/ψ] and the continuum processes ($q\bar{q}$, $q = u, d, s$) are incorporated in KKMC [22]. The known decay modes are generated using EVTGEN [23], which assumes the branching fractions reported in Ref. [13]; the fraction of unmeasured decays of charmonium states is generated with LUNDCHARM [24]. The final-state radiation (FSR) from charged tracks is simulated by the PHOTOS package [25]. A generic MC sample with equivalent luminosity 35 times that of data is generated to study the background. It contains open charm processes, the ISR return to charmonium states at lower mass, and continuum processes (quantum electrodynamics and $q\bar{q}$). The signal MC samples of 5.2 million $e^+e^- \to D_s^{*\pm}D_s^{\mp}$ events are produced; in these samples the $D_s^{*\pm}$ decays into $\gamma/\pi^0/e^+e^-D_s^{\pm}$, while one D_s decays into a specific mode in Table II and the other into the final states of interest $K_S^0K^{\pm}$ or $K_L^0K^{\pm}$. The signal MC samples are used to determine the distributions of kinematic variables and estimate the detection efficiencies.

III. DATA ANALYSIS

The cross section to produce $e^+e^- \to D_s^{*\pm}D_s^{\mp}$ events at $\sqrt{s} = 4.178$ GeV is $(889 \pm 59_{\rm stat.} \pm 47_{\rm syst.})$ pb, which is one order of magnitude larger than that to produce $e^+e^- \to D_s^+D_s^-$ events [14]. Furthermore, the decay branching fraction $\mathcal{B}(D_s^{*+} \to \gamma D_s^+)$ is $(93.5 \pm 0.7)\%$ [13]. Therefore, in the data sample used, D_s^+ candidates arise mainly from the process $e^+e^- \to D_s^{*\pm}D_s^{\mp} \to \gamma D_s^+D_s^-$, along with small fractions from the processes $e^+e^- \to D_s^{*\pm}D_s^{\mp} \to \pi^0 D_s^+D_s^-$ and $e^+e^- \to D_s^+D_s^-$. The outline of the reconstruction is described first, with all details given later in this section.

In this analysis, a sample of D_s^- mesons is reconstructed first, which are referred to as "single tag (ST)" candidates. The ST candidates are reconstructed in 13 hadronic decay modes that are listed in Table II. The $D_s^- \to K_S^0K^-$ tag mode is not included to avoid double counting in $D_s^+ \to K_S^0K^+$ measurement. Here, π^0 and η candidates are reconstructed from a pair of photon candidates, K_S^0 candidates are formed from $\pi^+\pi^-$ pairs, and $\rho^{\pm(0)}$ candidates are reconstructed from $\pi^{\pm}\pi^{0(\mp)}$ pairs, unless otherwise indicated by a subscript.

In the sample of events with ST candidates, the process $D_s^+ \to K_S^0K^+$ is reconstructed by selecting a charged kaon and a K_S^0 candidate from those not used to reconstruct the ST candidates, which is referred to as "double tag (DT)". To reconstruct the $D_s^+ \to K_L^0K^+$ decay, the photon from the decay $D_s^{*\pm} \to \gamma D_s^{\pm}$ and the charged kaon from D_s^+ decay are selected to determine the missing-mass-squared

$$MM^2 = (P_{e^+e^-} - P_{D_s^-} - P_\gamma - P_{K^+})^2, \qquad (2)$$

where $P_{e^+e^-}$ is the four-momentum of the e^+e^- initial state and $P_i (i = D_s^-, \gamma, K^+)$ is the four-momentum of the corresponding particle.

Ignoring the small contribution from the process $e^+e^- \to D_s^+D_s^-$, the numbers of ST ($N_{\rm ST}^i$) and DT ($N_{\rm DT}^i$) events, for a specific tag mode i, are

$$N^i_{\rm ST} = 2 \times N_{D^{*\pm}_s D^{\mp}_s} \times \mathcal{B}_{\rm tag}{}^i \times \epsilon^i_{\rm ST}, \quad (3)$$

$$N^i_{\rm DT} = 2 \times N_{D^{*\pm}_s D^{\mp}_s} \times \mathcal{B}_{\rm tag}{}^i \times \mathcal{B}_{\rm sig} \times \epsilon^i_{\rm DT}, \quad (4)$$

respectively. Here, $N_{D^{*\pm}_s D^{\mp}_s}$ is the total number of $e^+e^- \to D^{*\pm}_s D^{\mp}_s$ events in the data sample, $\mathcal{B}_{\rm tag}{}^i$ is the branching fraction for the ith ST decay mode, and $\mathcal{B}_{\rm sig}$ is the branching fraction of the signal decay; $\epsilon^i_{\rm ST}$ and $\epsilon^i_{\rm DT}$ are the ST and DT detection efficiencies, respectively, which are evaluated from the signal MC samples corresponding to the ith tag mode. The value of $\epsilon^i_{\rm DT}$ includes the branching fraction $\mathcal{B}(K^0_S \to \pi^+\pi^-)$ of the signal side in the analysis of $D^+_s \to K^0_S K^+$. The factors of 2 in Eqs. (3) and (4) are the result of including charge-conjugated modes in the analysis. We combine Eqs. (3) and (4) for each of the 13 tag modes to obtain

$$\mathcal{B}_{\rm sig} = \frac{N^{\rm tot}_{\rm DT}}{\sum_i N^i_{\rm ST} \times \epsilon^i_{\rm DT}/\epsilon^i_{\rm ST}}, \quad (5)$$

where $N^{\rm tot}_{\rm DT} = \sum_i N^i_{\rm DT}$ is the total number of DT events.

A. Selection of ST events

Good charged tracks, except for the daughter tracks of K^0_S candidates, are selected by requiring the track trajectory to approach the interaction point (IP) within ± 10 cm along the beam direction and within 1 cm in the plane perpendicular to the beam direction. In addition, the polar angle θ between the direction of the charged track and the beam direction must be within the detector acceptance by requiring $|\cos\theta| < 0.93$. Charged particle identification (PID) is performed by combining the ionization-energy loss ($\mathrm{d}E/\mathrm{d}x$) measured by the MDC and the time-of-flight measured by the TOF system. Each charged track is characterized by the PID likelihood for the pion and kaon hypotheses, which are $\mathcal{L}(\pi)$ and $\mathcal{L}(K)$, respectively. A pion (kaon) candidate is identified if it satisfies the condition $\mathcal{L}(\pi) > \mathcal{L}(K)$ $[\mathcal{L}(K) > \mathcal{L}(\pi)]$.

Good photon candidates are selected from isolated electromagnetic showers which have a minimum energy of 25 MeV in the EMC barrel region ($|\cos\theta| < 0.8$) or 50 MeV in the EMC end-cap region ($0.86 < |\cos\theta| < 0.92$). To reduce the number of photon candidates that result from noise and beam backgrounds, the time of the shower measured by the EMC is required to be less than 700 ns after the beam collision. The opening angle between a photon and the closest charged track is required to be greater than 10°, which is used to remove electrons, hadronic showers, and photons from FSR. π^0 and $\eta \to \gamma\gamma$ candidates are reconstructed from pairs of photon candidates that have an invariant mass within the intervals (0.115, 0.150) and $(0.50, 0.57)$ GeV/c^2, respectively. To improve the momentum resolution, a kinematic fit is performed, constraining the $\gamma\gamma$ invariant mass to its nominal value [13]; the χ^2 of the fit is required to be less than 20 to reject the combinatorial background. $\eta \to \pi^+\pi^-\pi^0$ candidates are selected by requiring the corresponding invariant mass to be within the interval (0.534, 0.560) GeV/c^2.

In order to improve the efficiency of the K^0_S selection, K^0_S candidates are reconstructed from tracks assumed to be pions without PID, and the daughter tracks are required to have a trajectory that approaches the IP to within ± 20 cm along the beam direction and $|\cos\theta| < 0.93$. The K^0_S candidates are formed by performing a vertex-constrained fit to all oppositely charged track pairs. To suppress combinatorial background, the χ^2 of the vertex fit is required to be less than 200 and a secondary vertex fit is performed to ensure that the K^0_S candidate originates from the IP. The flight length L, defined as the distance between the common vertex of the $\pi^+\pi^-$ pair and the IP in the plane perpendicular to the beam direction, is obtained in the secondary vertex fit, and is required to satisfy $L > 2\sigma_L$, where σ_L is the estimated uncertainty on L; this criterion removes the combinatorial background formed from tracks originating from the IP. The four-momenta after the secondary vertex fit are used in the subsequent analysis. The K^0_S candidate is required to have a mass within the interval $(0.487, 0.511)$ GeV/c^2.

η' candidates are reconstructed via the decay modes $\gamma\rho^0$ and $\pi^+\pi^-\eta$ by requiring the corresponding invariant masses to be within the intervals (0.936, 0.976) and $(0.944, 0.971)$ GeV/c^2, respectively. The ρ^0 candidates are reconstructed from $\pi^+\pi^-$ pairs that have a mass greater than 0.52 GeV/c^2. The $\rho^\pm$ candidates are reconstructed from $\pi^\pm\pi^0$ combinations that have an invariant mass within the interval $(0.62, 0.92)$ GeV/c^2.

To suppress the background with D^* decay $D^* \to \pi D$, the momentum of charged and neutral pions is required to be greater than 100 MeV/c. For $K^-\pi^+\pi^-$ ST candidates, the invariant mass of the $\pi^+\pi^-$ pair is required to be outside the interval $(0.478, 0.518)$ GeV/c^2 to remove $D^-_s \to K^0_S K^-$ decays. The ST D^-_s candidates are reconstructed via all the possible selected particle combinations.

The invariant mass of the system recoiling against the selected D^-_s is defined as

$$M_{\rm rec} = \sqrt{(\sqrt{s} - \sqrt{p^2 + M^2_{D_s}})^2 - p^2}, \quad (6)$$

where p is the momentum of the ST D^-_s candidate in e^+e^- CM frame, and M_{D_s} is the nominal mass of the D_s meson [13]. $M_{\rm rec}$ is required to be within the interval $(2.05, 2.18)$ GeV/c^2. For a specific ST mode, if there are multiple combinations satisfying the selection criteria, only the candidate with the minimum value of $|M_{\rm rec} - M_{D^*_s}|$ is retained for further analysis. These requirements also accept the events in which the ST D_s comes from the decay of the primary D^*_s.

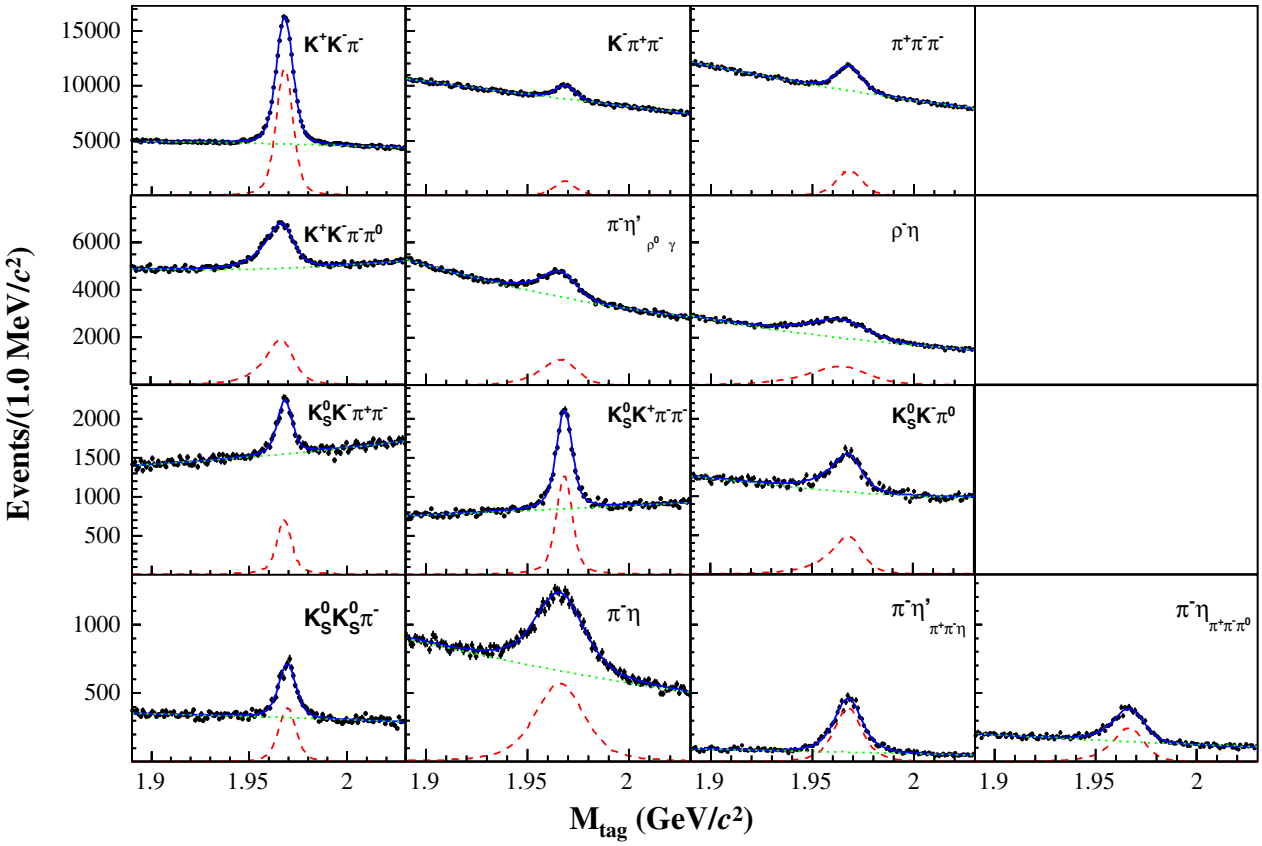

FIG. 1. Fits to $M_{\rm tag}$ distributions for each ST mode. The dots with error bars are data, the blue solid curves are the overall fit results, the red dashed curves are the signal, and the green dotted curves are the background.

To determine the ST yield, a binned maximum likelihood fit to the distribution of the D_s^- invariant mass $M_{\rm tag}$ is performed for each tag mode; the distributions and fit results are shown in Fig. 1. In the fit, the probability density function (PDF) that describes the signal is the shape of the signal MC distribution, taken as a smoothed histogram and convolved with a Gaussian function to account for any resolution difference between data and MC simulation. The background is described by a second- or third-order Chebyshev polynomial function. The ST yields determined by the fits, along with the corresponding $\epsilon_{\rm ST}^i$ estimated from the generic MC sample, are summarized in Table II.

B. Branching fraction measurement of $D_s^+ \to K_S^0 K^+$

The signal decay $D_s^+ \to K_S^0 K^+$ is reconstructed recoiling against the selected ST D_s^- candidate. We select a $D_s^+ \to K_S^0 K^+$ candidate if there is only one K_S^0 candidate and one good track, which is identified as a kaon and has positive charge, recoiling against the ST D_s^- candidate; K^+ and K_S^0 candidates are selected by applying the selection criteria described in Sec. III A. In addition, to suppress combinatorial backgrounds, we reject events in which there are additional charged tracks that satisfy $|\cos\theta| < 0.93$ and approach the IP along the beam direction within ± 20 cm.

To determine the DT signal yield, a two-dimensional (2D) unbinned maximum likelihood fit is performed on the invariant mass of the K_S^0 and K^+ ($M_{K_S^0 K^+}$) vs $M_{\rm tag}$ distribution of selected events, which is summed over the 13 ST modes, as shown in Fig. 2. In the fit, the total PDF is described by summing over the individual PDFs for the following signal and background components, where x represents $M_{K_S^0 K^+}$, and y stands for $M_{\rm tag}$.

(i) Signal: $F_{\rm sig}(x,y) \otimes G(x;\mu_x,\sigma_x) \otimes G(y;\mu_y,\sigma_y)$
$F_{\rm sig}(x,y)$ is a 2D function derived from the signal MC distribution by using a smoothed 2D histogram; $G(x;\mu_x,\sigma_x)$ and $G(y;\mu_y,\sigma_y)$ are Gaussian functions that compensate for any resolution difference between data and MC simulation for the variables $M_{K_S^0 K^+}$ and $M_{\rm tag}$, respectively. In the 2D fit, the parameters of $G(x;\mu_x,\sigma_x)$ and $G(y;\mu_y,\sigma_y)$ are fixed to the values determined by fitting the corresponding one-dimensional (1D) distributions.

(ii) BKGI: $F_{\rm BKGI}(x,y) \otimes G(y;\mu_y,\sigma_y)$
This PDF describes the background composed of a correctly reconstructed ST D_s^- recoiling against a combinatorial background, which are distributed in the horizontal band in Fig. 2. $F_{\rm BKGI}(x,y)$ is derived from the distribution of this type of background in

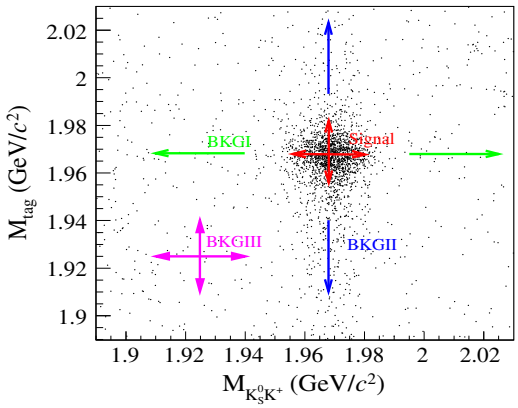

FIG. 2. Distribution of $M_{\rm tag}$ vs $M_{K^0_S K^+}$ for $D_s^+ \to K^0_S K^+$ candidates in data, summed over the 13 tag modes.

the generic MC sample by using a kernel density estimation method (KEYS) [26]. The resolution function $G(y;\mu_y,\sigma_y)$ is the same as that in the signal PDF.

(iii) BKGII: $F_{\rm BKGII}(x,y) \otimes G(x;\mu_x,\sigma_x)$
This PDF describes the background composed of an incorrectly reconstructed ST D_s^- recoiling against a correctly reconstructed signal candidate, which are distributed in the vertical band in Fig. 2. $F_{\rm BKGII}(x,y)$ is derived from the distribution of this type of background in the generic MC sample by using KEYS. The resolution function $G(x;\mu_x,\sigma_x)$ is the same as that in the signal PDF.

(iv) BKGIII: $P_{\rm BKGIII}(x) \times P_{\rm BKGIII}(y)$
This PDF describes the combinatorial background composed of events in which neither the ST D_s^- nor signal D_s^+ candidate is correctly reconstructed. These background events do not have any peaking components in either variable. Therefore, BKGIII events are described by two independent second-order polynomials, $P_{\rm BKGIII}(x)$ and $P_{\rm BKGIII}(y)$, with their parameters determined by the fit to data.

The 2D fit gives a signal yield of 1782 ± 47, where the uncertainty is statistical. The $M_{K^0_S K^+}$ and $M_{\rm tag}$ distributions for the data, with the projections of the fit results superimposed, are shown in Fig. 3. The corresponding DT detection efficiencies for the individual ST mode, obtained with the signal MC samples, are summarized in Table II. Using Eq. (5), the branching fraction is determined to be $\mathcal{B}(D_s^+ \to K^0_S K^+) = (1.425 \pm 0.038_{\rm stat.})\%$.

C. Branching fraction measurement of $D_s^+ \to K^0_L K^+$

The $D_s^+ \to K^0_L K^+$ candidates are reconstructed by requiring the event to have only one good track recoiling against the ST D_s^- candidate; the charged track is required to be identified as a kaon and have opposite charge

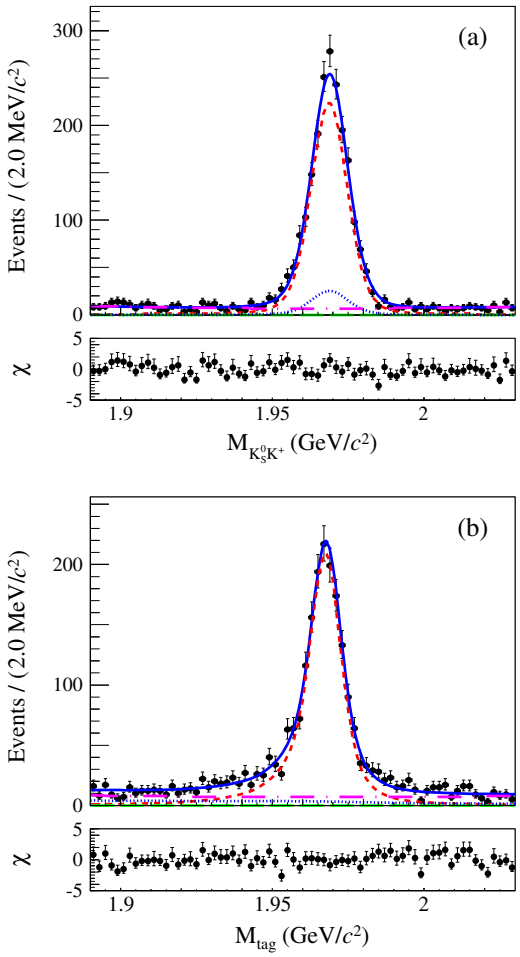

FIG. 3. (a) Distributions of $M_{K^0_S K^+}$ and (b) $M_{\rm tag}$, summed over the 13 tag modes, with the projection of the fit result superimposed. The data are shown as the black dots with error bars, the blue solid line is the total fit projection, the red short-dashed line is the projection of the signal component, the green long-dashed line is the projection of the BKGI component, the blue dotted line is the projection of the BKGII component, and the magenta dotted-dashed line is the projection of the BKGIII component. The residual χ between the data and the total fit result, normalized by the uncertainty, is shown beneath the figures.

compared with ST D_s^-. The K^+ is selected with the criteria described in Sec. III A. We further suppress combinatorial backgrounds by requiring no additional charged tracks that satisfy the requirements described in Sec. III B.

In this analysis, the ST and signal candidates are assumed to originate from the decay chain $e^+e^- \to D_s^{*\pm} D_s^{\mp} \to \gamma D_s^+ D_s^-$, with one D_s^- decaying into any of ST modes, and the other decaying into $K^0_L K^+$. We reconstruct the K^0_L candidate using a kinematic fit that applies constraints arising from the masses of the ST D_s^- candidate, the signal D_s^+ candidate, the intermediate state $D_s^{*\pm}$, and the initial four-momenta of the event. In the kinematic fit, the K^0_L signal candidate is treated as a missing particle whose four-momentum is determined by the fit. The fit is performed to

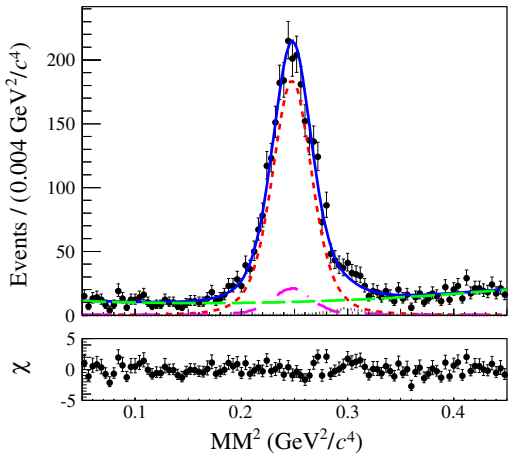

FIG. 4. Distribution of MM^2 summed over 13 tag modes with the fit result superimposed. The data are shown as the dots with error bars, the blue solid line is the total fit result, the red short-dashed line is the signal component of the fit, the magenta dotted-dashed line is the component of the peaking background from $D_s^+ \to K_S^0 K^+$ decays, the grey dotted line is the component of the peaking background from $D_s^+ \to \eta K^+$ decays, and the green long-dashed line is the nonpeaking background component. The residual χ between the data and the total fit result, normalized by the uncertainty, is shown beneath the figures.

select the γ candidate from the decay $D_s^{*\pm} \to \gamma D_s^{\pm}$ under two different hypotheses that constrain either the invariant mass of the selected γ and signal D_s^+ or the selected γ and the ST D_s^- to the nominal mass of the D_s^{*-} meson; the hypothesis that results in the minimum value of χ^2 is assumed to be the correct topology. If there are multiple photon candidates, which are not used to reconstruct the ST candidate, the fit is repeated for each candidate and the photon that results in the minimum value of the χ^2 is retained for further analysis. For each event, the four-momentum of the missing particle assumed in the kinematic fit is used to determine the MM^2 of the K_L^0 candidate. In order to reduce combinatorial background, $\chi^2 < 40$ is required. To further suppress background with multiple photons, we reject those events with additional photons which have an energy larger than 250 MeV and an opening angle with respect to the direction of the missing particle greater than 15°.

To determine the signal yield, an unbinned maximum likelihood fit is performed on the MM^2 distribution of selected events from all 13 ST modes combined, as shown in Fig. 4. In the fit, three components are included: signal, peaking, and nonpeaking backgrounds. The PDFs of these components are described below, where x represents MM^2.

(i) Signal: $F_{\rm sig}(x) \otimes G(x;\mu_x',\sigma_x')$

$F_{\rm sig}(x)$ is derived from the signal MC distribution as a smoothed histogram, and $G(x;\mu_x',\sigma_x')$ is a Gaussian function that accounts for any resolution difference between data and MC simulation. The value of σ_x' is fixed in the data fit to the value obtained from a fit to the MM^2 distribution obtained from a $D_s^+ \to K_S^0 K^+$ control sample where the K_S^0 is ignored in the reconstruction.

(ii) Peaking background: $F_{\rm bkg}^{K_S^0(\eta)}(x) \otimes G(x;\mu_x',\sigma_x')$

$F_{\rm bkg}^{K_S^0(\eta)}(x)$ is derived from the distribution of $D_s^+ \to K_S^0 K^+$ ($D_s^+ \to \eta K^+$) MC simulated events by using a smoothed histogram. These events form a peaking background if the K_S^0 or η is not reconstructed. Here, $G(x;\mu_x',\sigma_x')$ is the Gaussian resolution function, whose parameters are the same as those used in the signal PDF. The expected yields of $D_s^+ \to K_S^0 K^+$ and $D_s^+ \to \eta K^+$ are fixed to 263 and 57, respectively. The expected peaking background yields are estimated by using the equation $N_{MM^2}^{\rm data} = N_{\rm DT}^{\rm data} \times \epsilon_{MM^2}^{\rm MC}/\epsilon_{\rm DT}^{\rm MC}$, where $N_{MM^2}^{\rm data}$ is the number of expected peaking background events and $N_{\rm DT}^{\rm data}$ is the yield of $D_s^+ \to K_S^0 K^+$ or $D_s^+ \to K^+\eta$ selected by using the DT method. Here, $\epsilon_{MM^2}^{\rm MC}$ and $\epsilon_{\rm DT}^{\rm MC}$ are the detection efficiencies of the nominal analysis and the DT method for each mode, respectively; these are estimated from MC simulation samples. The uncertainties of estimated event numbers for $D_s^+ \to K_S^0 K^+$ and $D_s^+ \to \eta K^+$ are 19 and 12, which will be used in the systematic uncertainty study.

(iii) Nonpeaking background: $P(x)$

$P(x)$ is a function to describe the combinatorial background, which is not expected to peak in the MM^2 distribution. $P(x)$ is a second-order polynomial function whose parameters are determined from the fit to data.

The fit to the MM^2 distribution is shown in Fig. 4. The signal yield determined by the fit is 2349 ± 61 events, where the uncertainty is statistical. Using Eq. (5), the branching fraction is calculated to be $\mathcal{B}(D_s^+ \to K_L^0 K^+) = (1.485 \pm 0.039_{\rm stat.})\%$, where the DT detection efficiencies $\epsilon_{MM^2}^{K_L^0}$ used are summarized in Table II; the values of $\epsilon_{MM^2}^{K_L^0}$ are estimated from signal MC samples.

D. Asymmetry measurement

By using the measured branching fractions and Eq. (1) the K_S^0-K_L^0 asymmetry is determined to be

$$R(D_s^+ \to K_{S,L}^0 K^+) = (-2.1 \pm 1.9_{\rm stat.})\%. \quad (7)$$

To determine the direct CP violation, we also measure the branching fractions for the D_s^+ and D_s^- decays separately, using the same methodology as the combined branching fraction measurement. The direct CP asymmetry is defined as

$$A_{\rm CP}(D_s^{\pm}\to f)=\frac{\mathcal{B}(D_s^{+}\to f)-\mathcal{B}(D_s^{-}\to \bar{f})}{\mathcal{B}(D_s^{+}\to f)+\mathcal{B}(D_s^{-}\to \bar{f})}, \quad (8)$$

which leads to the measurements

$$A_{\rm CP}(D_s^{\pm}\to K_S^0K^{\pm})=(0.6\pm 2.8_{\rm stat.})\%, \quad (9)$$

$$A_{\rm CP}(D_s^{\pm}\to K_L^0K^{\pm})=(-1.1\pm 2.6_{\rm stat.})\%, \quad (10)$$

for the two signal modes.

IV. SYSTEMATIC UNCERTAINTY

For the absolute branching fractions, which are determined according to Eq. (5), the systematic uncertainties are associated with $N^i_{\rm ST}$, $N^{\rm tot}_{\rm DT}$, and the corresponding ratio of detection efficiencies ($\epsilon^i_{\rm DT}/\epsilon^i_{\rm ST}$). One of the advantages of the DT method is that most of the systematic uncertainties associated with selection criteria for the ST side reconstruction cancel. However, there is some residual uncertainty due to the different decay topologies between DT and ST events; this is referred to as "tag-side bias," and its effect is considered as one of the systematic uncertainties. For the $R(D_s^+)$ and $A_{\rm CP}$ measurements, the systematic uncertainties are calculated by propagating corresponding branching fraction uncertainties from different sources taking into account that some of the uncertainties cancel due to the fact that these observables are ratios as defined in Eqs. (1) and (8).

Table III summarizes the relative uncertainties on the absolute branching fraction and the absolute uncertainties for the asymmetries. The total systematic uncertainties are calculated as the sum in quadrature of individual contributions by assuming the sources are independent of one another.

The K^+ and K^- tracking efficiencies are studied using a control sample of $e^+e^-\to K^+K^-\pi^+\pi^-$ events; the efficiency is calculated as a function of the transverse momentum of the particles. The average efficiency difference between data and MC is computed to be 0.5% by weighting the efficiency difference found in the control sample according to the transverse momentum of the kaon in signal MC samples. This is assigned as the systematic uncertainty from this source.

The K^+ and K^- PID efficiencies are studied using a control sample of $D_s^+\to K^+K^-\pi^+$, $D^0\to K^-\pi^+$ and $D^0\to K^-\pi^-\pi^+\pi^+$ events; the efficiency is calculated as a function of the momentum of the particle. The average efficiency difference between data and MC is computed to be 0.5% by weighting the efficiency difference found in the control sample according to the momentum of the kaon in signal MC samples, and this is assigned as the systematic uncertainty from this source.

The K_S^0 reconstruction efficiency has been studied using control samples of $J/\psi\to K^*(892)^{\mp}K^{\pm}$ and $J/\psi\to \phi K_S^0K^{\pm}\pi^{\mp}$ in different momentum intervals [27]. The efficiency difference between data and MC is computed to be 1.5%, which is assigned as the systematic uncertainty from this source.

The systematic uncertainty associated with the photon selection efficiency and the kinematic fit in the study of $D_s^+\to K_L^0K^+$ is estimated from the control sample $D_s^+\to K^+K^-\pi^+$. The same kinematic fit as that used on the data is performed by assuming the $K^-\pi^+$ system is missing. The efficiency difference found between data and MC simulation, 2.0%, is taken as the systematic uncertainty.

The systematic uncertainties associated with the requirements on the energy of additional photons and the number of extra charged tracks are estimated from the control sample $D_s^+\to K^+K^-\pi^+$. The efficiency differences

TABLE III. Summary of relative systematic uncertainties (%) of the branching fraction measurements and the absolute systematic uncertainties (%) of the $A_{\rm CP}$ and $R(D_s^+)$ measurements.

Source	$\mathcal{B}(D_s^+\to K_S^0K^+)$	$\mathcal{B}\,(D_s^+\to K_L^0K^+)$	$R(D_s^+\to K^0_{S,L}K^+)$	$A_{\rm CP}(D_s^{\pm}\to K_S^0K^{\pm})$	$A_{\rm CP}(D_s^{\pm}\to K_L^0K^{\pm})$
K^+/K^- tracking	0.5	0.5	···	0.4	0.4
K^+/K^- PID	0.5	0.5	···	0.4	0.4
K_S^0 reconstruction	1.5	···	0.7	···	···
Photon selection and kinematic fit	···	2.0	1.0	···	···
Extra photon energy requirement	···	0.6	0.3	···	···
Extra charged track requirement	0.6	0.6	···	···	···
ST $M(D_s)$ fit	0.9	0.9	···	···	···
DT fit	0.8	···	0.4	···	···
MM^2 fit	···	1.5	0.7	···	···
MC statistics	0.3	0.3	0.2	0.2	0.2
Effect of $\mathcal{B}(D_s^*\to\gamma D_s)$	···	0.7	0.3	···	···
Effect of $e^+e^-\to D_s^+D_s^-$	···	0.4	0.2	···	···
Tag-side bias	0.3	0.5	0.3	···	···
Total	2.2	3.1	1.6	0.6	0.6

between data and MC simulation for these two requirements are both 0.6%, which are assigned as the systematic uncertainties from these sources.

The uncertainty related to the limited sizes of MC samples is 0.3% for both $D_s^+ \to K_S^0 K^+$ and $D_s^+ \to K_L^0 K^+$.

The uncertainties associated with ST, DT, and MM^2 fits are studied by changing the signal and background PDFs, as well as the fit interval; each change is applied separately. Furthermore, in the MM^2 fit, the effect of the assumed peaking background yields is estimated by changing the fixed numbers of events by $\pm 1\sigma$. The systematic uncertainties related to the ST, DT, and MM^2 fit procedure are 0.9%, 0.8% and 1.5%, respectively; these are the sums in quadrature of the relative changes of signal yield that result from each individual change to the fit procedure.

As discussed previously, the selected ST D_s^- sample is dominated by the process $e^+e^- \to D_s^{*\pm} D_s^{\mp} \to \gamma D_s^+ D_s^-$, but there is a small contribution from the processes $e^+e^- \to D_s^{*\pm} D_s^{\mp} \to \pi^0 D_s^+ D_s^-$ and $e^+e^- \to D_s^+ D_s^-$. In the analysis of $D_s^+ \to K_S^0 K^+$, detailed MC studies indicate that $\epsilon_{\rm DT}^i/\epsilon_{\rm ST}^i$ is almost the same for the three processes, since distributions of the kinematic variables are similar and no kinematic fit is performed in the DT selection. Thus, the effect from including $e^+e^- \to D_s^{*\pm} D_s^{\mp} \to \pi^0 D_s^+ D_s^-$ and $e^+e^- \to D_s^+ D_s^-$ processes is negligible in the absolute branching fraction measurement. In the analysis of $D_s^+ \to K_L^0 K^+$, the kinematic fit is performed under the hypothesis that the event is $e^+e^- \to D_s^{*\pm} D_s^{\mp} \to \gamma D_s^+ D_s^-$, and the MC studies indicate that the contribution of $e^+e^- \to D_s^{*\pm} D_s^{\mp} \to \pi^0 D_s^+ D_s^-$ and $e^+e^- \to D_s^+ D_s^-$ in signal events can be neglected. Thus, the uncertainty of the branching fraction $\mathcal{B}(D_s^{*+} \to \gamma D_s^+)$ [13] used in the signal MC simulation must be taken as a source of systematic uncertainty. The systematic uncertainty from excluding the process $e^+e^- \to D_s^+ D_s^-$ is 0.4%, which is the fraction of the ST yields that comes from the process $e^+e^- \to D_s^+ D_s^-$; this fraction is estimated from the MC simulation.

The tag-side bias uncertainty is defined as the uncanceled uncertainty in the tag side due to different track multiplicities in generic and signal MC samples. By studying the differences of tracking and PID efficiencies between data and MC in different multiplicities, the tag-side bias systematic uncertainties are estimated to be 0.3% for $D_s^+ \to K_S^0 K^+$ and 0.5% for $D_s^+ \to K_L^0 K^+$.

V. SUMMARY AND DISCUSSION

In summary, by using an e^+e^- collision data sample at $\sqrt{s} = 4.178$ GeV, corresponding to an integrated luminosity of 3.19 fb^{-1}, the absolute branching fractions are measured to be $\mathcal{B}(D_s^+ \to K_S^0 K^+) = (1.425 \pm 0.038_{\rm stat.} \pm 0.031_{\rm syst.})\%$ and $\mathcal{B}(D_s^+ \to K_L^0 K^+) = (1.485 \pm 0.039_{\rm stat.} \pm 0.046_{\rm syst.})\%$; the former is one standard deviation lower than the world average value [13], and the latter is measured for the first time. The K_S^0-K_L^0 asymmetry in D_s^+ decay is measured for the first time as $R(D_s^+ \to K_{S,L}^0 K^+) = (-2.1 \pm 1.9_{\rm stat.} \pm 1.6_{\rm syst.})\%$. This measurement is compatible with theoretical predictions listed in Table I. Direct CP asymmetries of the two processes are obtained to be $A_{\rm CP}(D_s^\pm \to K_S^0 K^\pm) = (0.6 \pm 2.8_{\rm stat.} \pm 0.6_{\rm syst.})\%$ and $A_{\rm CP}(D_s^\pm \to K_L^0 K^\pm) = (-1.1 \pm 2.6_{\rm stat.} \pm 0.6_{\rm syst.})\%$. No significant asymmetries are observed and the uncertainties are statistically dominant.

ACKNOWLEDGMENTS

The BESIII collaboration thanks the staff of BEPCII and the IHEP computing center, and the supercomputing center of USTC for their strong support. This work is supported in part by National Key Basic Research Program of China under Contract No. 2015CB856700; National Natural Science Foundation of China (NSFC) under Contracts No. 11335008, No. 11375170, No. 11475164, No. 11475169, No. 11605196, No. 11605198, No. 11625523, No. 11635010, No. 11705192, No. 11735014, No. 11822506, No. 11835012; the Chinese Academy of Sciences (CAS) Large-Scale Scientific Facility Program; Joint Large-Scale Scientific Facility Funds of the NSFC and CAS under Contracts No. U1532102, No. U1532257, No. U1532258, No. U1732263, No. U1832103, No. U1832207; CAS Key Research Program of Frontier Sciences under Contracts No. QYZDJ-SSW-SLH003, No. QYZDJ-SSW-SLH040; 100 Talents Program of CAS; INPAC and Shanghai Key Laboratory for Particle Physics and Cosmology; ERC under Contract No. 58462; German Research Foundation DFG under Contracts No. Collaborative Research Center CRC 1044, No. FOR 2359; Istituto Nazionale di Fisica Nucleare, Italy; Koninklijke Nederlandse Akademie van Wetenschappen (KNAW) under Contract No. 530-4CDP03; Ministry of Development of Turkey under Contract No. DPT2006K-120470; National Science and Technology fund; The Knut and Alice Wallenberg Foundation (Sweden) under Contract No. 2016.0157; The Royal Society, UK under Contracts No. DH140054, No. DH160214; The Swedish Research Council; U. S. Department of Energy under Contracts No. DE-FG02-05ER41374, No. DE-SC-0010118, No. DE-SC-0012069; University of Groningen (RuG) and the Helmholtzzentrum fuer Schwerionenforschung GmbH (GSI), Darmstadt. WCU Program of National Research Foundation of Korea under Contract No. R32-2008-000-10155-0.

[1] L. L. Chau, Phys. Rep. **95**, 1 (1983).
[2] L. L. Chau and H. Y. Cheng, Phys. Rev. Lett. **56**, 1655 (1986).
[3] I. I. Y. Bigi and H. Yamamoto, Phys. Lett. B **349**, 363 (1995).
[4] F. S. Yu, D. Wang, and H. n. Li, Phys. Rev. Lett. **119**, 181802 (2017).
[5] Z. Z. Xing, Phys. Rev. D **55**, 196 (1997).
[6] T. Gershon, J. Libby, and G. Wilkinson, Phys. Lett. B **750**, 338 (2015).
[7] B. Bhattacharya and J. L. Rosner, Phys. Rev. D **81**, 014026 (2010).
[8] H. Y. Cheng and C. W. Chiang, Phys. Rev. D **81**, 074021 (2010).
[9] S. Müller, U. Nierste, and S. Schacht, Phys. Rev. D **92**, 014004 (2015).
[10] D. N. Gao, Phys. Rev. D **91**, 014019 (2015).
[11] D. Wang, F. S. Yu, P. F. Guo, and H. Y. Jiang, Phys. Rev. D **95**, 073007 (2017).
[12] Q. He *et al.* (CLEO Collaboration), Phys. Rev. Lett. **100**, 091801 (2008).
[13] M. Tanabashi *et al.* (Particle Data Group), Phys. Rev. D **98**, 030001 (2018).
[14] D. Cronin-Hennessy *et al.* (CLEO Collaboration), Phys. Rev. D **80**, 072001 (2009).
[15] P. U. E. Onyisi *et al.* (CLEO Collaboration), Phys. Rev. D **88**, 032009 (2013).
[16] A. Zupanc *et al.* (Belle Collaboration), J. High Energy Phys. 09 (2013) 139.
[17] C. H. Yu *et al.*, in *Proceedings of IPAC2016, Busan, Korea, 2016*, http://dx.doi.org/10.18429/JACoW-IPAC2016-TUYA01.
[18] X. Wang *et al.* J. Instrum. **11**, C08009 (2016).
[19] M. Ablikim *et al.* (BESIII Collaboration), Nucl. Instrum. Methods Phys. Res., Sect. A **614**, 345 (2010).
[20] S. Agostinelli *et al.* (GEANT4 Collaboration), Nucl. Instrum. Methods Phys. Res., Sect. A **506**, 250 (2003).
[21] R. G. Ping, Chin. Phys. C **38**, 083001 (2014).
[22] S. Jadach, B. F. L. Ward, and Z. Was, Phys. Rev. D **63**, 113009 (2001); Comput. Phys. Commun. **130**, 260 (2000).
[23] D. J. Lange, Nucl. Instrum. Methods Phys. Res., Sect. A **462**, 152 (2001); R. G. Ping, Chin. Phys. C **32**, 599 (2008).
[24] J. C. Chen, G. S. Huang, X. R. Qi, D. H. Zhang, and Y. S. Zhu, Phys. Rev. D **62**, 034003 (2000).
[25] E. Richter-Was, Phys. Lett. B **303**, 163 (1993).
[26] K. S. Cranmer, Comput. Phys. Commun. **136**, 198 (2001).
[27] M. Ablikim *et al.* (BESIII Collaboration), Phys. Rev. D **92**, 112008 (2015).